Supplementary Figures

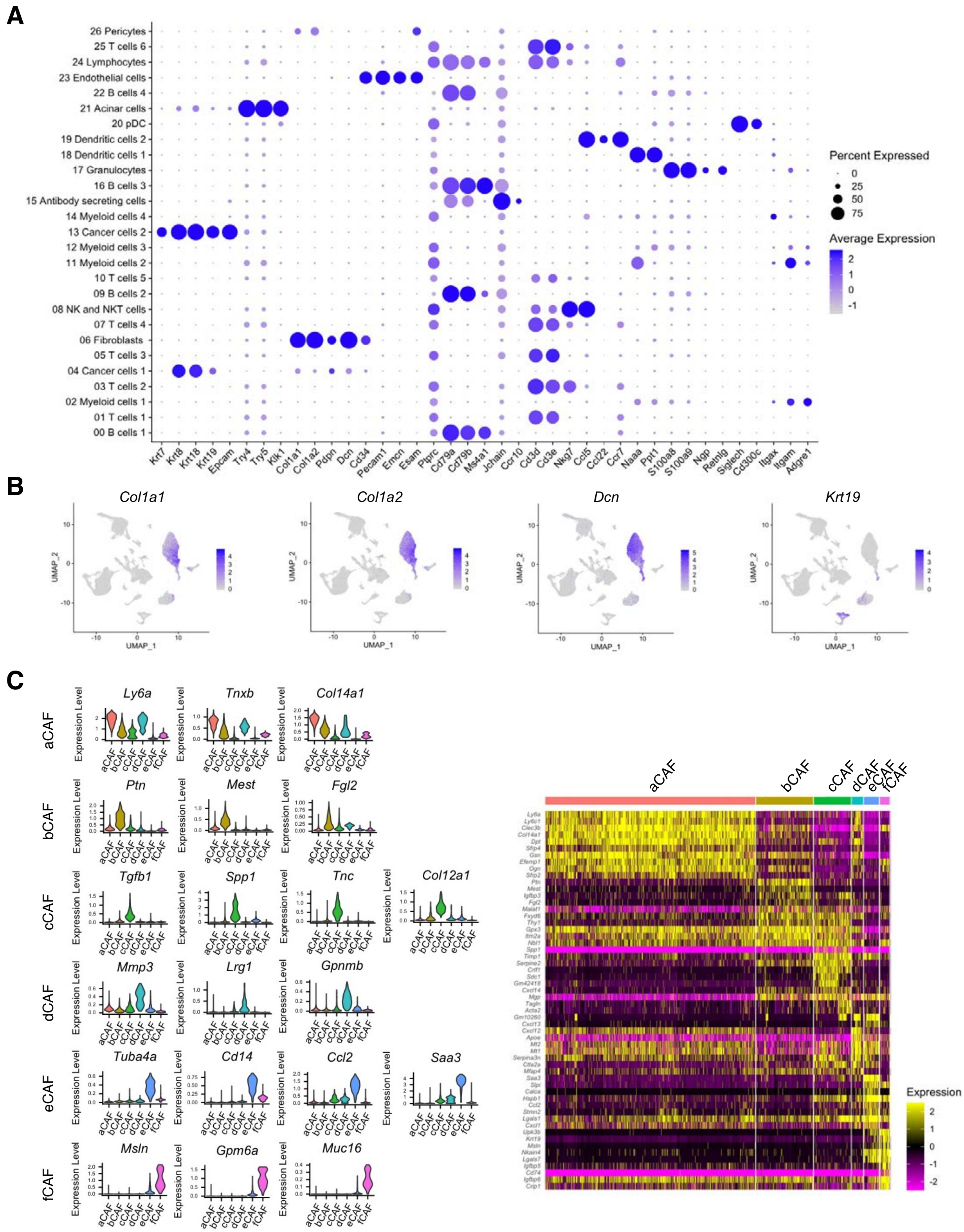

Supplementary Figure 1. Transcriptional definitions of cells in KPC tumors

(**A**) Dot plot of genes associated with the cell clusters identified by scRNA-seq of KPC tumors originally shown in Figure 1. n=8 mice, 31,861 cells.

(**B**) UMAP projection of cell populations in KPC tumors with the indicated relative gene expression. n=8 mice, 31,861 cells.

(**C**) Violin plots of gene expression levels in each CAF cluster identified in **Figure 1A**. aCAF: red, bCAF: yellow, cCAF: green, dCAF: teal, eCAF: blue, fCAF: magenta. Heatmap of genes associated with CAF clusters (right panel). Yellow: high expression levels, magenta: low expression levels. n=8 mice; 7,624 cells.

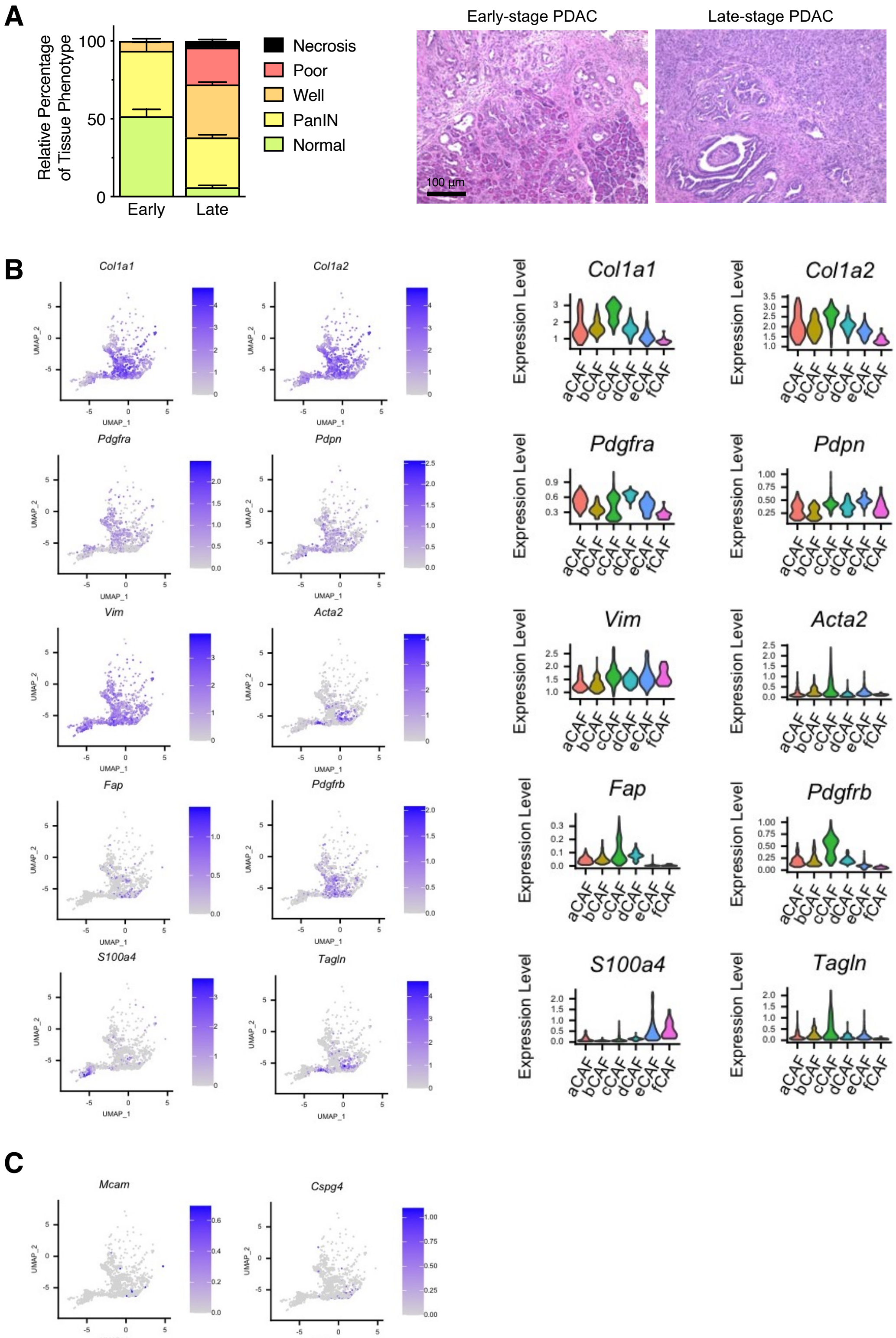

Supplementary Figure 2. Histology and expression of fibroblast and pericyte genes of CAFs in KPC tumors

(**A**) Relative percentages of each tumor histological phenotype in early-stage PDAC and late-stage PDAC of KPC mice (n=3 mice per group, left panel). PDAC samples with less than 10% pancreatic adenocarcinoma areas were defined as early-stage PDAC, while PDAC samples with greater than 50% pancreatic adenocarcinoma areas were defined as late-stage PDAC. Representative H&E staining images of early-stage and late-stage KPC tumors (right panel). Scale bar: 100 μm.

(**B**) UMAP projection of cell populations in late-stage KPC CAFs with the indicated relative gene expression (left panels) originally shown in Figure 1. Violin plots of the same genes indicating relative gene expression by cluster (right panels). n=3 mice; 1,606 cells.

(**C**) UMAP projections of common pericyte markers *Mcam* and *Cspg4* in KPC CAFs with the indicated relative gene expression. n=3 mice; 1,606 cells.

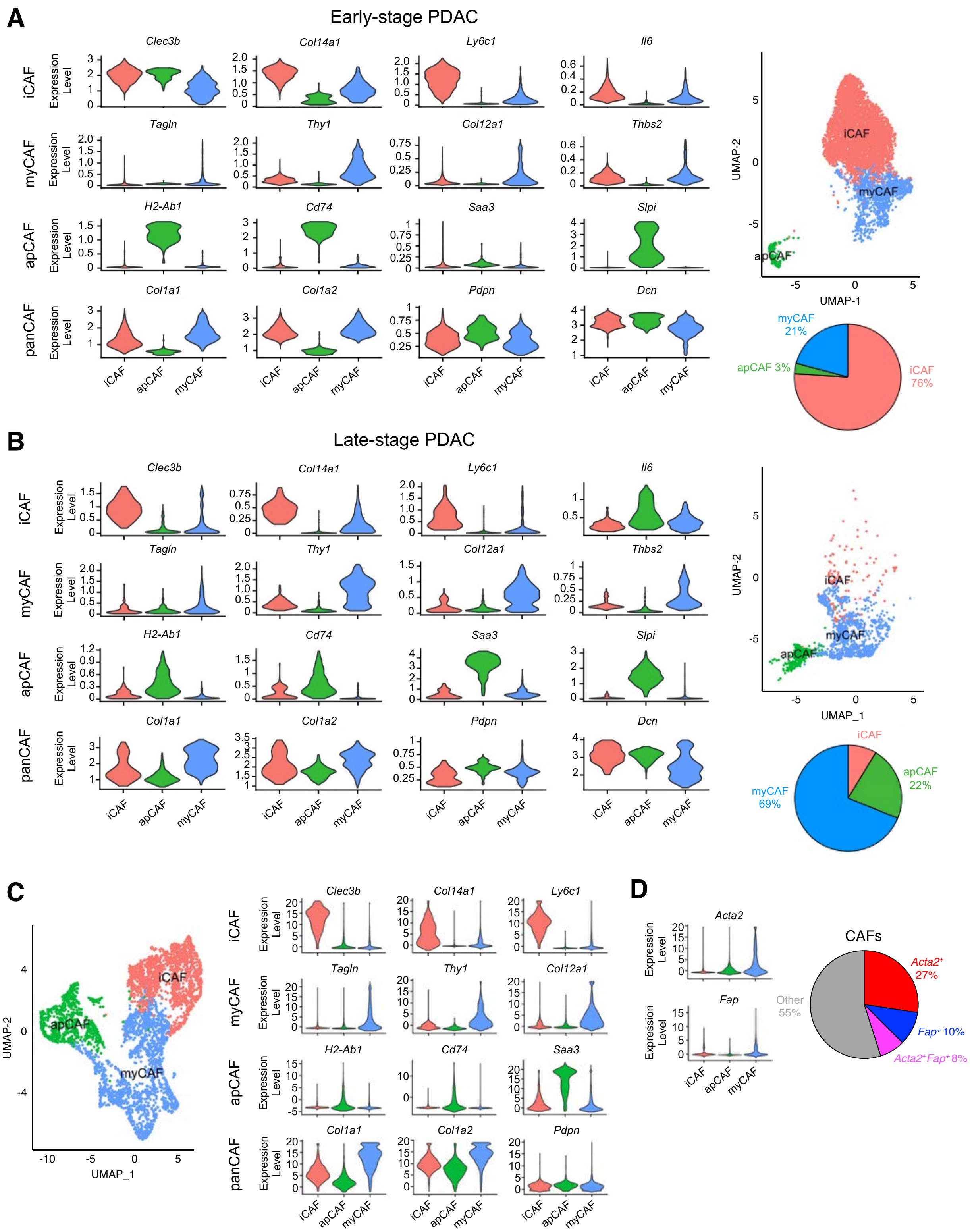

Supplementary Figure 3. Clustering of myCAF, iCAF, and apCAF in KPC tumors

(**A**) Violin plots (left panels), UMAP projections (top right panel), and percentages of iCAF, apCAF, myCAF, and panCAF genes (bottom right panel) in early-stage KPC tumors originally shown in Figure 1. n=5 mice; 6,018 cells.

(**B**) Violin plots (left panels), UMAP projections (top right panel), and percentages of iCAF, apCAF, myCAF, and panCAF genes (bottom right panel) in late-stage KPC tumors. n=3 mice; 1,606 cells.

(**C**) UMAP projections and violin plots of iCAF, myCAF, and apCAF of previously reported KPC tumors (16).

(**D**) Violin plots (left panels) and relative percentages (right panel) of *Acta2* and *Fap* in previously reported KPC tumors (16).

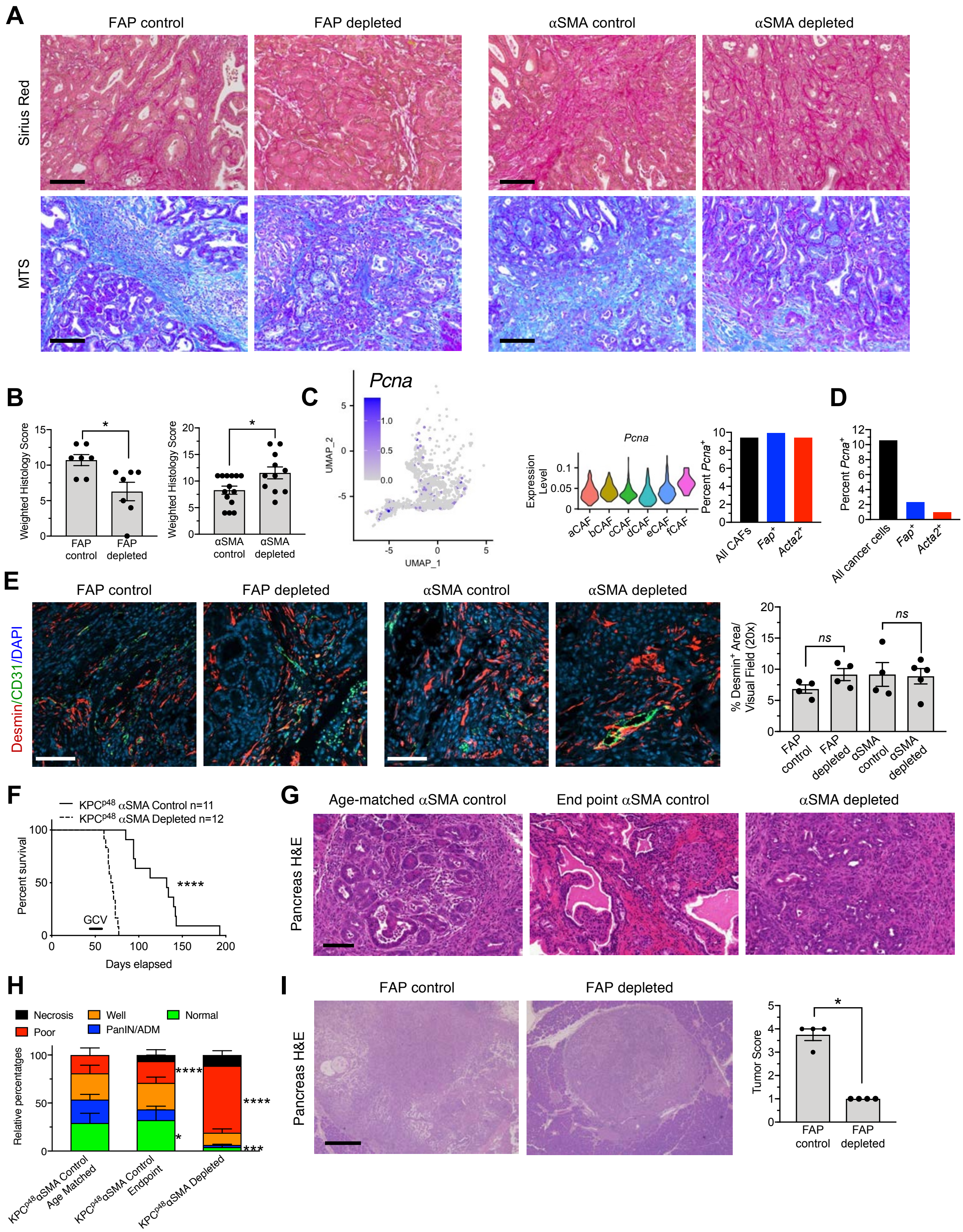

Supplemental Figure 4. Distinct effects on survival and PDAC progression with FAP^{+} CAF-depletion and αSMA^{+} CAF- depletion in KTC tumors

(**A**) Representative Sirius Red and MTS staining of KTC tumors. Scale bar: 100 μm.

(**B**) Quantification of weighted histology of KTC tumors. n=7 mice per group. Unpaired two-tailed t-test performed comparing FAP control to FAP depleted, Mann-Whitney test comparing αSMA control to αSMA depleted.

(**C**) UMAP projection (left panel) and violin plots (center panel) of *Pcna* in CAFs of late stage KPC mice originally shown in Figure 1. Percentage of CAFs positive for *Pcna* (right panel). n=3 mice; 1,606 cells.

(**D**) Percentage of cancer cells expressing *Pcna*, *Acta2*, and *Fap*.

(**E**) Representative CD31 (green) and desmin (red) co-staining of KTC tumors (left panel). Scale bar: 100 μm. Desmin pericyte tissue coverage in KTC tumors (right panel). FAP control, n=4 mice; FAP depleted, n=4 mice; αSMA control, n=4 mice; αSMA depleted, n=5 mice. The mean ± s.e.m. is depicted with Welch's two-tailed t-test comparing control to depleted mice performed.

(**F**) Survival curve of KPC^{p48} mice with and without $αSMA^+$ CAF-depletion. The bar indicates when GCV treatment was initiated. KPC^{p48} control, n=11 mice; KPC^{p48} αSMA depleted, n=12 mice. Log rank test performed.

(**G**) Representative H&E staining of pancreatic tumor sections of KPC^{p48} mice, with age-matched or end point controls. Scale bar: 100 μm.

(**H**) Relative percentages of each tumor histological phenotype (right panel). Age matched-control, n=7; endpoint control, n=11; $αSMA^+$ CAF-depleted, n=12 mice. Statistical significance was evaluated using two-way ANOVA comparing age-matched control to endpoint control and depleted mice.

(**I**) Representative H&E staining of pancreatic tumor sections of orthotopically implanted 689KPC cells in FAP-TK mice (left panel). Scale bar: 100 μm. Tumor score evaluated based on H&E staining (right panel, n=4 mice per group). The mean ± s.e.m. is depicted with a Mann-Whitney test performed comparing control to depleted mice. * $p < 0.05$, *** $p < 0.001$, **** $p < 0.0001$, *ns*: not significant.

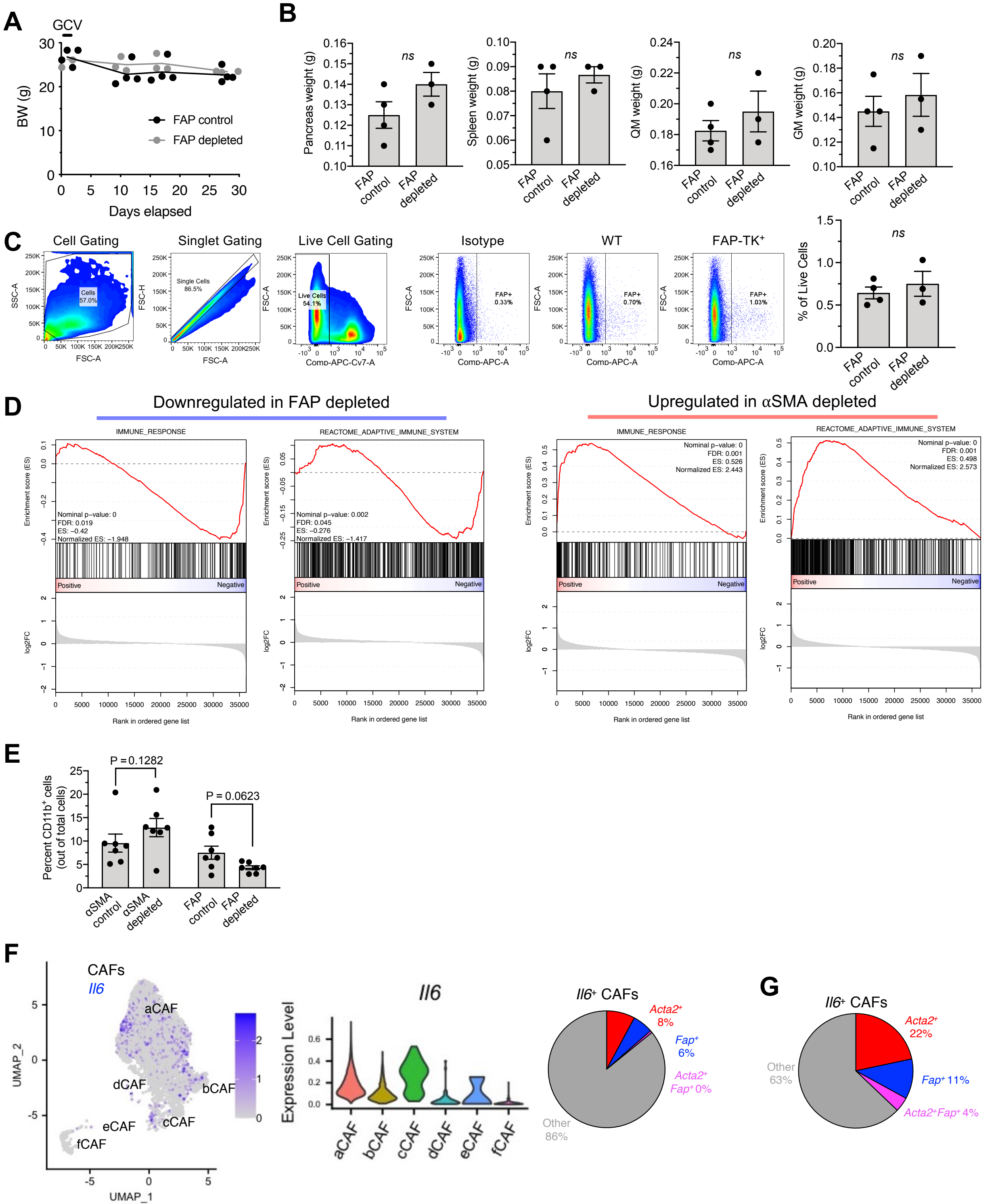

Supplemental Figure 5. Phenotypic changes in FAP^{+} CAF-depleted mice

(**A**) Body weight measurement over time in non-tumor bearing FAP-TK mice administered GCV. FAP control, n=4; FAP^{+} CAF-depleted, n=3 mice.

(**B**) Pancreas, spleen, quadriceps muscle (QM), and gastrocnemius muscle (GM) weight at end point. FAP control, n=4; FAP^+ CAF-depleted, n=3 mice. Mann-Whitney test performed. *ns*: not significant.

(**C**) Gating strategy and quantification of FAP^+ cells in the spleen. FAP control, n=4; FAP^+ CAF-depleted, n=3 mice. Unpaired two-tailed t-test performed. *ns*: not significant.

(**D**) Continued from Figure 4. GSEA revealing oppositely regulated pathways in FAP^+ CAF-depleted and αSMA^+ CAF-depleted KTC tumors. Top pathways are shown, which are downregulated in FAP^+ CAF-depleted KTC tumors and upregulated in αSMA^+ CAF-depleted KTC tumors. n=3 mice in each group.

(**E**) Continued from Figure 4. Quantification of percent $CD11b^+$ cells. n=7 mice in each group. One-way ANOVA and unpaired two-tailed t-test performed comparing control to depleted mice. Exact p-values shown.

(**F**) Continued from Figure 5A. The expression profile of *Il6* of CAF populations from early-stage KPC pancreatic tumors, presented in UMAP projection (left panel), violin plots (center panel), and percentages (right panel) as determined by scRNA-seq originally shown in Figure 1. n=5 mice; 6,018 cells.

(**G**) Continued from Supplementary Figure 3C. UMAP projections (left panel), violin plots (center panel), and relative percentage of *Il6* of previously reported KPC tumors (16).

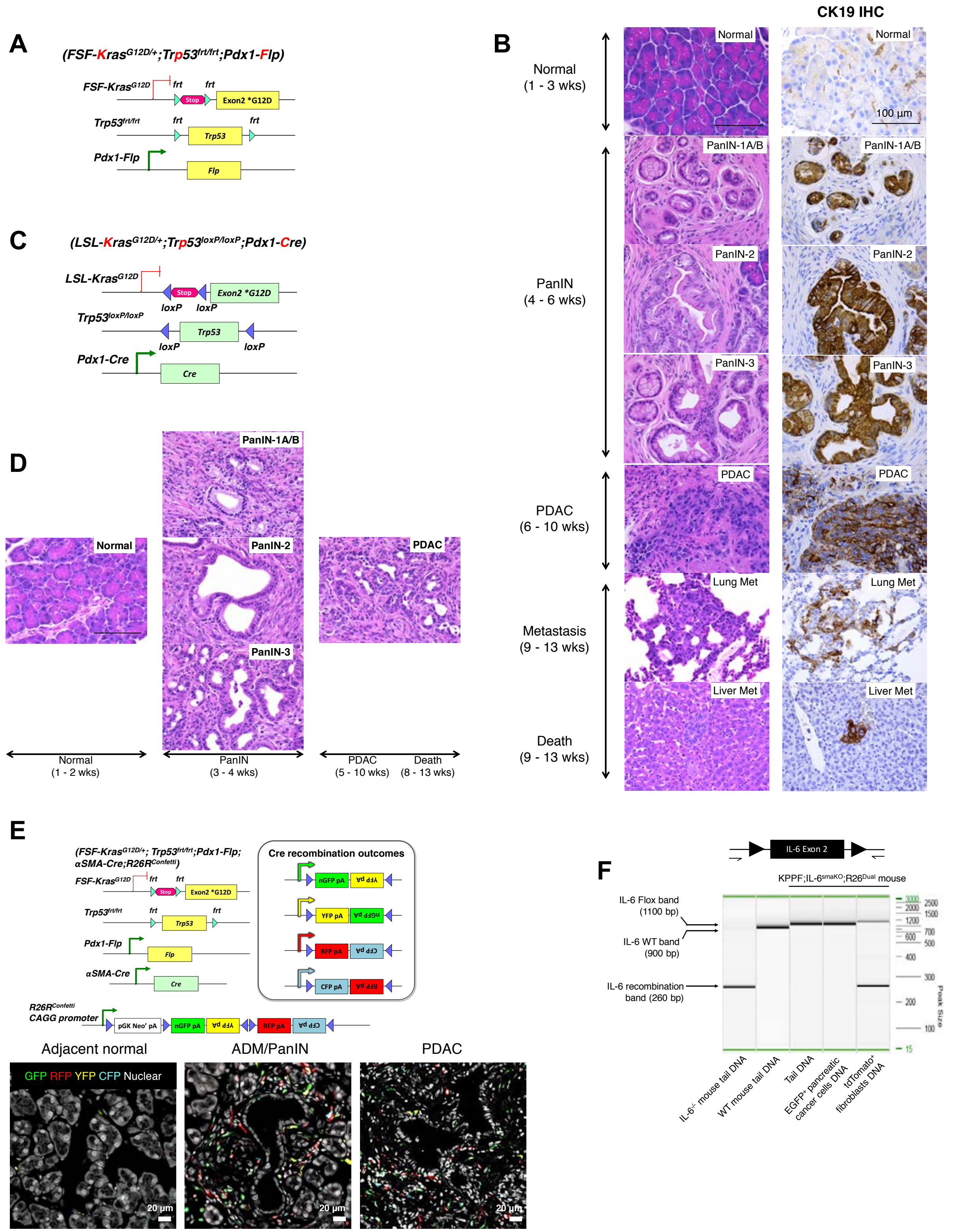

Supplementary Figure 6. Characterization of KPPF (*FSF-Kras$^{G12D/+}$;Trp53$^{frt/frt}$;Pdx1-Flp*) mice

(**A**) Genetic strategy to induce oncogenic *Kras*^{G12D} together with homozygous *Trp53* loss using the *Pdx1-Flp-FRT* recombination system in KPPF mice.

(**B**) Representative H&E-stained or CK19 immunostained sections of PanIN (stage 1-3), PDAC, and metastasis of KPPF mice. Scale bar: 100 μm.

(**C**) Genetic strategy to induce oncogenic *Kras*^{G12D} together with homozygous *Trp53* loss using the *Pdx1-Cre-loxP* recombination system in KPPC mice, which are genetically analogous to KPPF mice.

(**D**) Representative sections of PanIN (stage 1-3) and PDAC of KPPC mice stained by H&E.

Scale bars, 100 μm.

(**E**) Characterization of KPPF;αSMA-Cre;R26$^{\text{Confetti}}$ mice. Schematic illustrating the generation of KPPF;αSMA-Cre;R26$^{\text{Confetti}}$ mice by crossing the *R26R-Confetti* multicolor reporter allele with the *αSMA-Cre* and *KPPF* alleles. Representative immunofluorescence images of intrinsic GFP (green), YFP (yellow), RFP (red), CFP (cyan), and DRAQ5 nuclear staining (grey) in pancreatic tissue sections from KPPF;αSMA-Cre;R26$^{\text{Confetti}}$ mice. Scale bar, 20 μm.

(**F**) Electrophoretic migration of PCR products of purified DNA confirming the specific genetic deletion of IL-6 in CAFs (but not in PDAC cells) from KPPF;IL-6$^{\text{smaKO}}$;R26$^{\text{Dual}}$ mice.

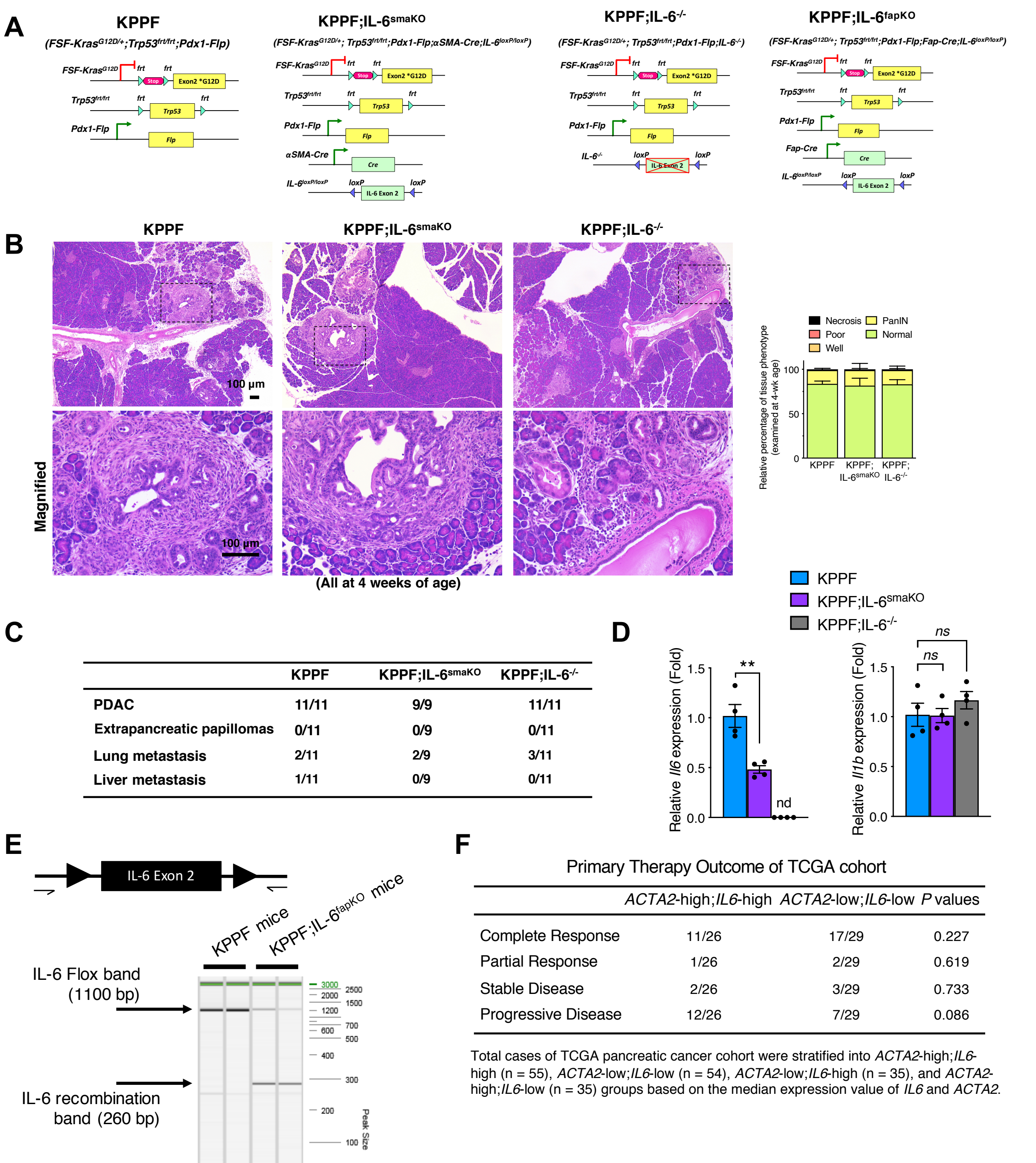

Supplementary Figure 7. Characterization of KPPF mice with either αSMA^{+} CAF-specific or whole-body IL-6 deletion

(**A**) Genetic strategy to delete IL-6 specifically in αSMA^{+} CAFs (KPPF;IL-6^{smaKO}), FAP^{+} CAFs (KPPF;IL-6^{fapKO}), or at the whole-body level (KPPF;IL-6$^{-/-}$) in KPPF mice.

(**B**) Representative pancreatic sections with H&E staining of KPPF, KPPF;IL-6^{smaKO}, and KPPF;IL-$6^{-/-}$ mice examined at 4 weeks of age and relative percentage of each histological tissue phenotype, continued from Figure 5G. n=3 mice per group. Scale bars, 100 µm. Two-way ANOVA with Tukey's multiple comparison test performed.

(**C**) Incidence of PDAC, papillomas, lung metastasis, and liver metastasis of KPPF, KPPF;IL-6^{smaKO}, and KPPF;IL-$6^{-/-}$ mice.

(**D**) Relative expression (mRNA abundance) of IL-6 (*Il6*), or IL-1β (*Il1b*), in PDAC tissues from KPPF, KPPF;IL-6^{smaKO}, and KPPF;IL-$6^{-/-}$ mice. Expression relative to *Gapdh* and KPPF tumors reported. n=4 biological replicates per group. For *Il6*: unpaired two-tailed t-test performed comparing KPPF to KPPF;IL-6^{smaKO}. For *Il1b*: One-way ANOVA with Dunnett's multiple comparisons test performed comparing KPPF;IL-6^{smaKO} and KPPF;IL-$6^{-/-}$ to KPPF. Statistical tests were performed based on ΔC_T values. nd: not detected. ** $p < 0.01$, *ns*: not significant.

(**E**) Electrophoretic migration of PCR products of purified DNA confirming the specific genetic deletion of IL-6 in ear tissues from KPPF;IL-6^{fapKO} mice, but not KPPF control mice.

(**F**) TCGA pancreatic cancer patients (n = 179) were stratified into *ACTA2*-high;*IL6*-high (n = 55), *ACTA2*-low;*IL6*-low (n = 54), *ACTA2*-low;*IL6*-high (n = 35), and *ACTA2*-high;*IL6*-low (n = 35) groups based on the median expression value of *IL6* and *ACTA2*. Statistical comparisons were evaluated with Chi-square test.

A

Metastases examined at end-stage

	KPPF Gem	KPPF;IL-6^{smaKO} Gem
Lung metastasis	2/10	2/10
Liver metastasis	1/10	0/10

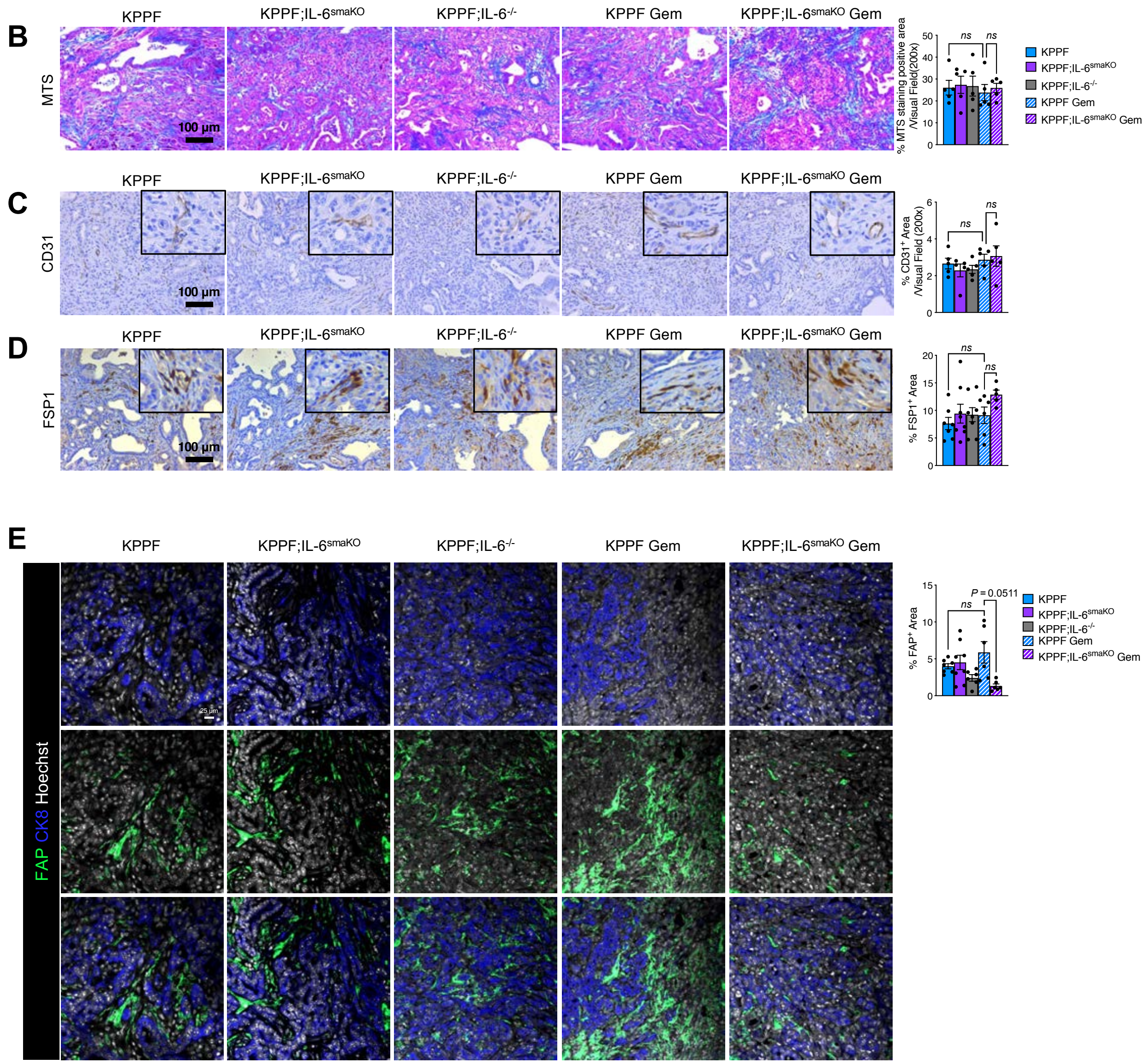

Supplementary Figure 8. Evaluation of the microenvironment of PDAC with IL-6 loss and treated with gemcitabine.

(**A**) Incidence of metastasis in KPPF and KPPF;IL-6^{smaKO} mice treated with gemcitabine.

(**B-D**) Representative sections of PDAC tissues from KPPF, KPPF;IL-6^{smaKO}, or KPPF;IL-6$^{-/-}$ mice with or without gemcitabine treatment, stained with Masson's trichrome stain (MTS, **B**), CD31 (**C**), and FSP1 (**D**).

n = 5 mice per group for (B) and (C). For (D): KPPF, n=7; KPPF;IL-6^{smaKO}, n=8; KPPF;IL-6$^{-/-}$, n=8; KPPF Gem, n=6; KPPF;IL-6^{smaKO} Gem, n=5. One-way ANOVA with Sidak's multiple comparison test performed. Scale bar: 100 µm.

(**E**) Representative images of PDAC tissues from KPPF, KPPF;IL-6^{smaKO}, or KPPF;IL-6$^{-/-}$ mice with or without gemcitabine treatment, stained with FAP and CK8 (cytokeratin-8, cancer cell marker) and quantification of FAP^{+} area. Scale bar, 25 µm. KPPF, n= 7; KPPF;IL-6^{smaKO}, n=8; KPPF;IL-6$^{-/-}$, n=6; KPPF Gem, n=6; KPPF;IL-6^{smaKO} Gem, n=6. Brown-Forsythe ANOVA with Dunnett's T3 multiple comparisons test performed. *ns*: not significant.

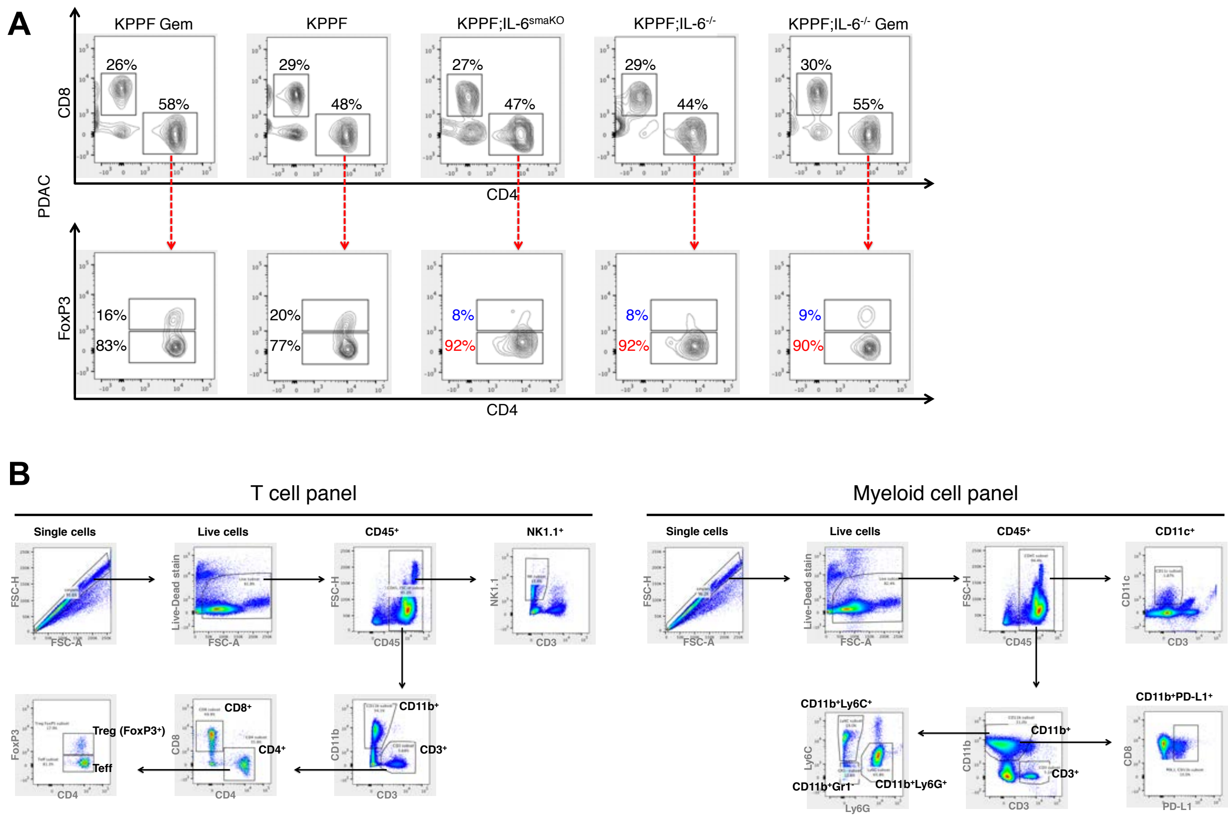

Supplementary Figure 9. Flow cytometry analyses of immune cells in PDAC with IL-6 loss and/or gemcitabine treatment

(**A**) Gating strategies for Treg cells in tumors with indicated genotypes and treatments.

(**B**) Gating strategies for flow cytometry analyses for T cell panel and myeloid cell panel.

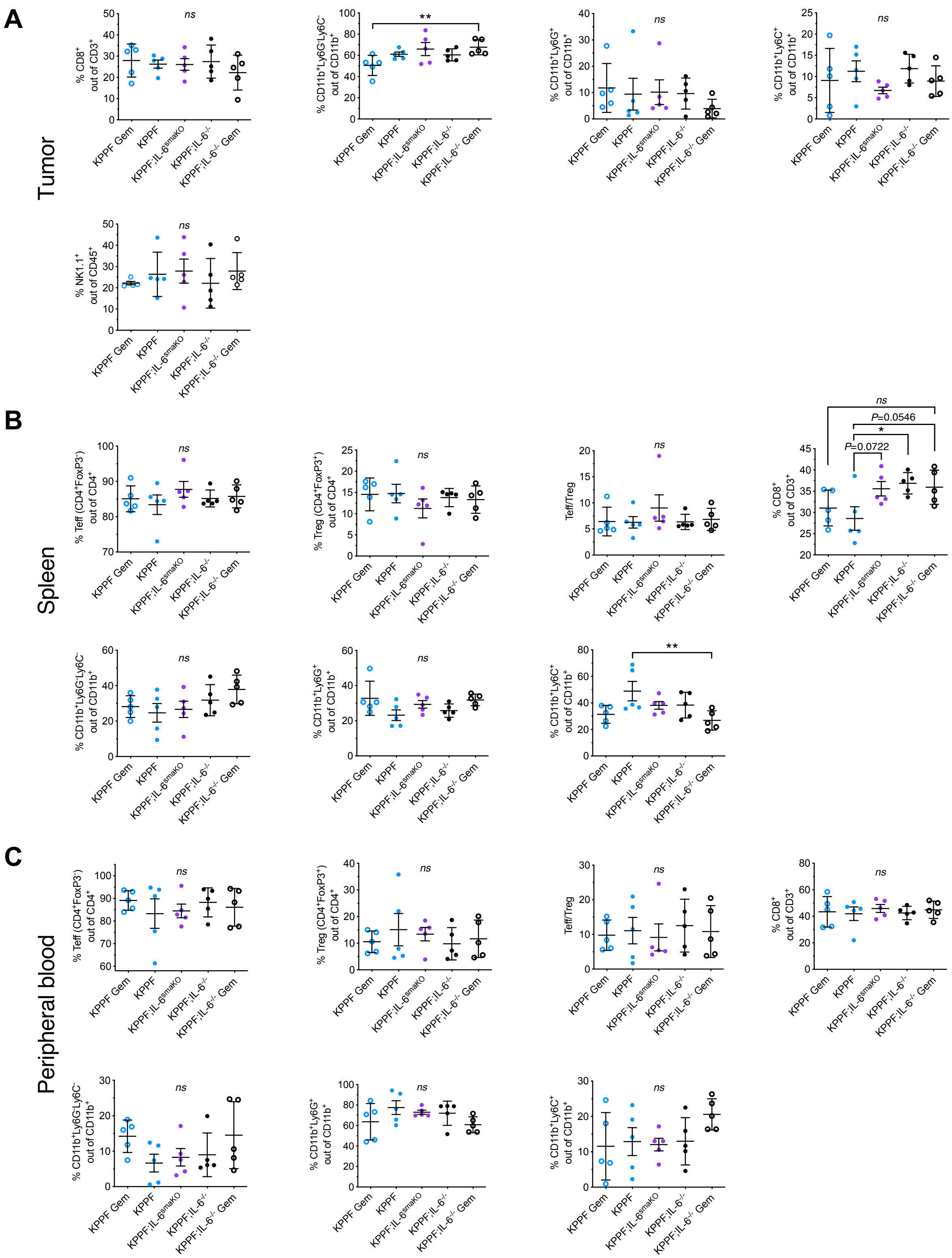

Supplementary Figure 10. PDAC immune infiltration modulated by IL-6 deletion

(**A-C**) Continued from Figure 6F. Single-cell suspensions of PDAC tumors (**A**), spleens (**B**), or peripheral blood (**C**) from indicated mouse groups (n = 5 mice per group, examined at 2.5-month age after saline or gemcitabine treatment for 2 weeks) were stained, examined by flow cytometry, and gated by live-dead stain, CD45, CD3, CD8, CD4, FoxP3, CD11b, Ly6G, Ly6C, PD-L1, CD11c, and NK1.1. The percentage of $CD4^+$ or $CD8^+$ cells among $CD3^+$ cells was calculated. The percentage of $CD4^+FoxP3^+$ regulatory T cells (Treg) or $CD4^+FoxP3^-$ effector T cells (Teff) among $CD4^+$ cells was calculated. Percentages of $CD11b^+Ly6G^-Ly6C^-$, $CD11b^+Ly6G^+$, $CD11b^+Ly6C^+$, $CD11b^+PD\text{-}L1^+$, $CD11c^+$, and $NK1.1^+$ cells are also shown. One-way ANOVA with Sidak's multiple comparison test performed for $CD8^+$, $CD11b^+Ly6G^-Ly6C^-$, and $CD11b^+Ly6G^+$ and Brown-Forsythe and Welch ANOVA with Dunnett's T3 performed for $CD11b^+Ly6C^+$ and $NK1.1^+$ in (A). Brown-Forsythe and Welch ANOVA with Dunnett's T3 performed for Teff/Treg and one-way ANOVA with Sidak's multiple comparison test performed for all other data in (B). One-way ANOVA with Sidak's multiple comparison test performed for (C). * $p < 0.05$, ** $p < 0.01$, *ns*: not significant.